THE PENNSYLVANIA STATE UNIVERSITY
SCHREYER HONORS COLLEGE

DEPARTMENT OF BIOLOGY

The Role of Tca-17 in Cellulose Synthase Complex Trafficking in *Arabidopsis thaliana*

JENNA PATEL
SPRING 2024

A thesis
submitted in partial fulfillment
of the requirements
for a baccalaureate degree
in Biology Vertebrate Physiology
with honors in Biology

Reviewed and approved* by the following:

Ying Gu
Professor of Biochemistry and Molecular Biology
Thesis Supervisor

Stephen W. Schaeffer
Professor of Biology
Honors Adviser

* Electronic approvals are on file.

ABSTRACT

Plant cell walls are essential for a plant's growth, development, and structural integrity towards biological and environmental factors. Cellulose is one of the main structural components in the primary cell walls of plants. This biopolymer is synthesized at the plasma membrane by cellulose synthase complexes (CSC), which are made up of cellulose synthase proteins (CESA). Previous research has shown that CSC complexes and CESA proteins are found in the plasma membrane during synthesis; however, the assembly and trafficking of these complexes to the membrane are poorly understood. In this study, we investigate the role Tca17, a TRAPPII and TRAPPIII specific subunit, may play in regulating CSC dynamics and compare its subcellular dynamics to Trs85, a TRAPPIII specific subunit. We found that *tca17* mutants had reduced seven-day-old dark-grown hypocotyls and a lower crystalline cellulose content in four-day-old hypocotyls. The YFP-CESA6 density at the plasma membrane in *prc1-1 tca17* was not affected in 2.5-day-old etiolated hypocotyls, unlike the increase in YFP-CESA6 density observed in *prc1-1 trs85-1*. Overall, our findings suggest that Tca17 is involved in cellulose synthesis at the plasma membrane, however, the role it plays may be different and independent of Trs85.

TABLE OF CONTENTS

LIST OF FIGURES

ACKNOWLEDGEMENTS

I would like to express my sincere gratitude to the Gu Lab for their invaluable support, guidance, and resources for the past couple of years. The enriching educational and research experience I gained from the lab has significantly contributed to my academic and personal development throughout my undergraduate journey. I would also like to extend my appreciation to Holly Allen and Dr. Ying Gu for their constant advice and encouragement during the execution of my thesis project. Overall, I am grateful for the time and dedication invested by the entire Gu Lab team in nurturing my research skills and knowledge.

Chapter 1

Introduction

1.1. Cellulose Overview in *Arabidopsis thaliana*

Cellulose is the most abundant biopolymer on Earth that is gaining attention due to its economic potential as a source for renewable biofuels and sustainable products (Allen *et al.*, 2021). Research also suggests that cellulose may serve as a carbon sink on Earth, potentially playing a role in reducing climate change (Ezquer *et al.*, 2020). In plants, cellulose is a linear β-1,4 linked D-glucan chain that forms microfibrils via intermolecular and intramolecular hydrogen bonds (Endler *et al*., 2015). It is a crucial structural component of the primary cell walls in plants, providing the plants with the mechanical strength to withstand external environmental forces. Therefore, understanding the mechanisms behind the synthesis of cellulose in the primary cell walls is important for maintaining plant resilience and advancing research in this promising field.

The primary cell wall in plants is comprised of three main polymers: cellulose, hemicellulose, and pectin (Allen *et al.*, 2021). While most of the plant cell polysaccharides, both hemicellulose and pectin, are synthesized at the Golgi and secreted to the apoplast, cellulose is synthesized at the plasma membrane by cellulose synthase complexes (CSC) in *Arabidopsis thaliana* (Zhang *et al*., 2015). The newly growing cellulose microfibrils extrude from the CSCs and are inserted into the apoplast (Lei *et al*., 2015). Each CSC is arranged in a hexameric rosette structure, comprising of six subunits with each subunit housing three cellulose synthase proteins (CESA) (Endler *et al*., 2015; Allen *et al.*, 2021). For the primary cell walls, CESA1, CESA3, and CESA6/6 are essential for cellulose synthesis (Allen *et al.*, 2021). While CESA proteins are synthesized in the endoplasmic reticulum (ER), the assembly and trafficking of the CSC complexes to the plasma membrane are not well understood (Zhang *et al*., 2015). Exploring this topic allows one to gain a comprehensive understanding of cellulose synthesis in *Arabidopsis thaliana*.

1.2. The Function of the TRAPP Complex

Intracellular transportation of proteins and lipids from one organelle to another relies on vesicles to carry the newly synthesized macromolecules to their correct location. These vesicles go through four processes to allow the contents within the vesicle to reach their desired organelle and function properly: budding from the donor compartment, targeting, tethering, and fusion with the acceptor compartment (Kim *et al.*, 2016). Rab GTPases play a pivotal role in controlling intracellular trafficking pathways; they aid the vesicles in transitioning from the tethering phase to the fusion phase with the acceptor compartment. TRAPP complexes are guanine exchange factors (GEFs) that help activate Rab GTPases. The complexes will catalyze the generation of the GTP-bound form of Rab, thus activating the protein (Ravikumar *et al.*, 2017). Therefore, TRAPP complexes serve as important proteins to investigate in regard to its regulation of the intracellular trafficking pathway.

The function and composition of the TRAPP complexes in *Arabidopsis thaliana* are not well understood; however, TRAPP complexes are highly conserved protein complexes also found in yeast and mammals, which serve as model organisms to allow researchers to learn more about the complex's role in plants (Kim *et al.*, 2016). In yeast, there are three distinct TRAPP complexes — TRAPPI, TRAPPII, and TRAPPIII — each of which are GEFs that activate Rab Ypt1 and have distinct roles in the secretory pathway (Figure 1). TRAPPII is thought to function within the Golgi and TGN/EE-PM trafficking while TRAPPIII is thought to be involved in the autophagy process (degradation of parts of the cell through lysosomes) (Barrowman *et al.*, 2010). TRAPP complex's interaction with Rab GTPases creates a connection to the trafficking pathway and allows us to investigate its possible role in the transportation of CSC from the Golgi to the plasma membrane.

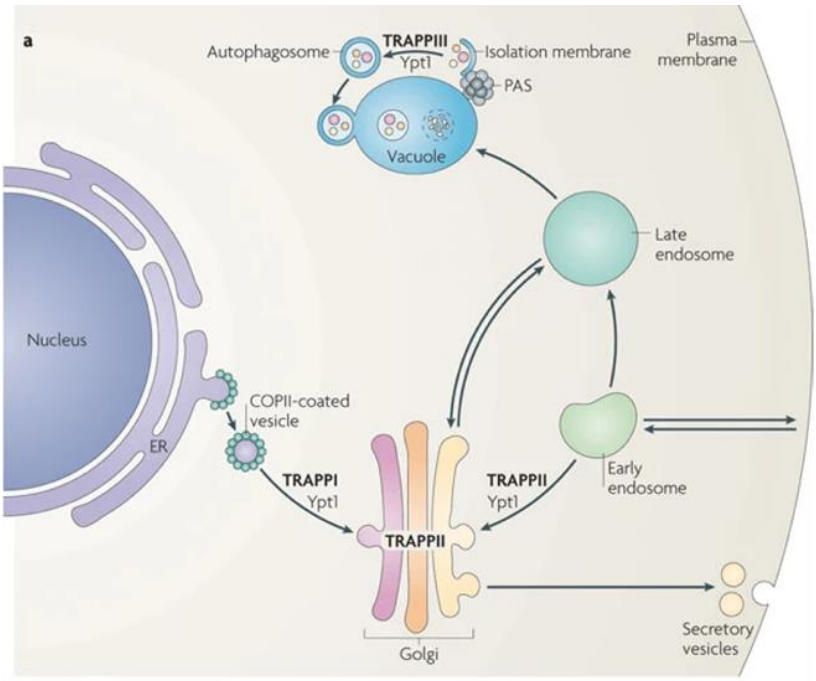

Figure 1. TRAPP Complexes Functions in the Trafficking Pathway in Yeast

Each TRAPP complex has a different function in the trafficking pathway in yeasts. TRAPPI is found to help mediate ER-to-Golgi transport. TRAPPII is thought to function within the Golgi and play a role in the TGN/EE-PM trafficking. TRAPPIII is involved with autophagy at vacuoles. Each of the complexes is a guanine exchange factor that interacts with the Rab GTPase, Ypt1 (Barrowman *et al.*, 2010).

1.3. Tca17 Specific Subunit of TRAPP Complex

As previously mentioned, the composition of the TRAPP complexes in *Arabidopsis thaliana* is not known. However, by looking at the TRAPP complexes in yeast and mammals, a proposed model of the TRAPP complexes in plants can be created (Figure 2). Each of the TRAPP complexes has a common core of seven subunits. These seven subunits alone make up TRAPPI, which is also known as Core TRAPP. In addition to the common core subunits, TRAPPII and TRAPPIII have different accessory subunits that aid in their specific function. Tca17 is a subunit found in both TRAPPII and TRAPPIII. It is

a Sedlin_N family member that is similar to the TRAPP subunit Trs20 (Montpetit and Conibear, 2009). Previous research has shown that Tca17 is a novel binding partner of the TRAPP complex. The loss of Tca17 can lower the association of the TRAPPII subunits, leading to the suggestion that Tca17 plays a role in maintaining the complex composition, assembly, or stability (Montpetit and Conibear, 2009).

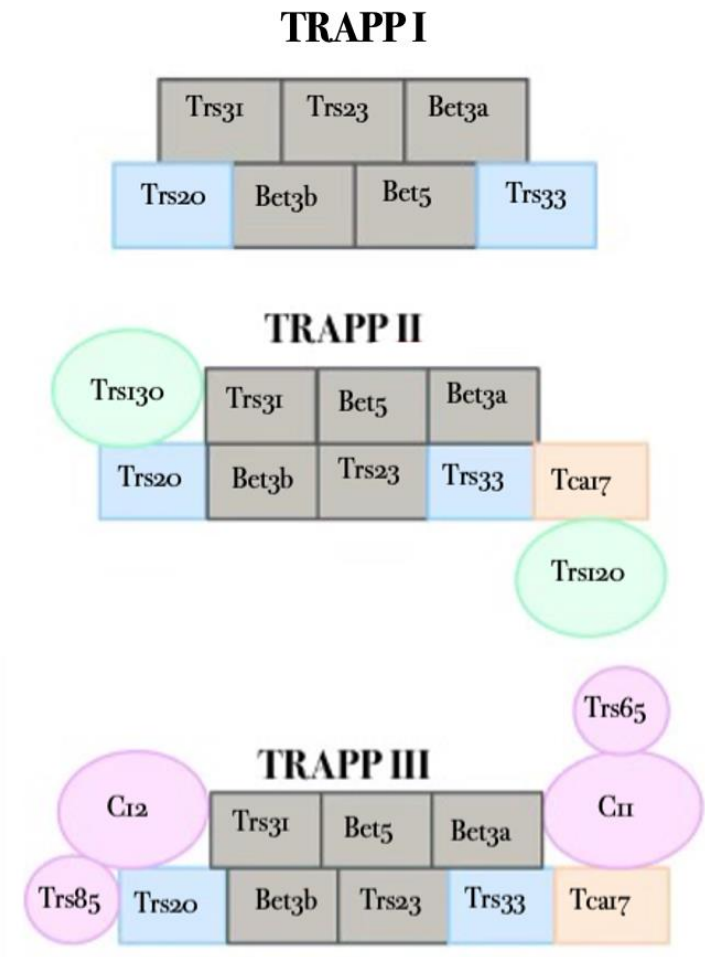

Figure 2. Proposed Composition of TRAPP Complexes in *Arabidopsis thaliana*

The composition and arrangement of TRAPPI (Core TRAPP), TRAPP II, and TRAPPIII are shown in this Figure. The grey and blue subunits represent the seven core subunits found in each TRAPP complex. The green subunits are the accessory subunits found only in TRAPPII. The pink subunits are specific accessory subunits found in TRAPPIII only. The orange subunit, Tca17, is found in both TRAPPII and TRAPPIII.

1.4. Overall Goal of Research Project

This research aims to explore if the TRAPPII and TRAPIII-specific subunit, Tca17, plays a role in the trafficking of CSC within the endomembrane system and to the plasma membrane for cellulose synthesis. DNA genotyping, hypocotyl length analyses, RNA expression, and crystalline cellulose content assays will be collected on four different subunits —*tca17, rog2-2, bet3*, and *trs65*— within the TRAPPII and TRAPPIII complex to determine if the subunits influence the cellulose production in the primary cell wall. Toward the latter part of the research, there will be an increased focus on the Tca17 subunit and the dynamics of the CESA6 particles in the *tca17* mutant background. Currently, the function and role in cellulose production of Tca17 is unknown; however, I hypothesize Tca17 has a similar density of CESA6 particles at the plasma membrane to the Trs85 subunit, a TRAPPIII specific subunit, and thus a similar role as Trs85.

Chapter 2

Materials and Methods

2.1. Experimental Design Overview

This study will begin with a DNA expression analysis on the *tca17*, *rog2-2*, *trs65*, and *bet3* mutants to confirm their homozygosity. Subsequently, hypocotyl length analyses will be carried out on four-day-old and seven-day-old dark-grown hypocotyls for the *tca17*, *rog2-2*, *trs65*, and *bet3* mutants to assess any cellulose-related phenotypes. To explain the hypocotyl length phenotypes, gene expression for each mutant will be determined. If a cellulose-related phenotype manifests in a mutant, a cellulose content assay will be performed on the mutant to determine if a disruption in cellulose synthesis is present. Finally, the subcellular density dynamics of YFP-CESA6 particles will be investigate in the *tca17* mutant via confocal microscopy live cell imaging using the Yokogawa CSUX1 spinning disk system.

2.2. Plant Materials and Growth Conditions

Arabidopsis thaliana seeds were placed into a 1.5 mL Eppendorf tube, sterilized with 1 mL 30% bleach, washed six times with 1 mL sterilized double distilled water, and stored at 4 ºC for 72 hours. For dark-grown conditions, the seeds were grown on plates containing ½ Murashige and Skoog (MS) and 0.05% 2-(N-morpholino)ethanesulfonic acid (MES), exposed to the light for 2 hours, wrapped in aluminum foil, and grown vertically at 22 ºC in darkness for the desired number of days. For light-grown conditions, the seeds were plated on MS plates (½ MS, 0.05% MES, and 1% sucrose) for the desired number of days. To collect seeds from adult plants, seven-day-old seedlings were transplanted into soil and grown at 22 ºC under a 16-h light/8-h cycle for 6-8 weeks. When half the plant began to turn yellow, the plants were placed outside the chamber to fully dry before collecting the seeds.

2.3. Hypocotyl Length Measurement

Four-day and seven-day-old seedlings were scanned, and Fiji-ImageJ was used to measure the hypocotyl of the etiolated four-day and seven-day seedlings. The hypocotyl lengths for each mutant and control group were averaged. A one-way ANOVA test was conducted to compare the means of each mutant to wild type (Col-0), the negative control, and *csi1-3*, the positive control. The statistical comparative analysis was performed using Prism 10.

2.4. DNA Extraction

A two-week-old *Arabidopsis thaliana* leaf was placed in a -80 ºC freezer for 30 minutes. Then, the leaf was grounded and suspended in 400 µl of Edwards buffer (10 mL 1M Tris pH 8.0, 2.5 mL 5M NaCl, 2.5 mL 0.5M EDTA pH 8.0, 1.25 mL 20% SDS) for 10 minutes on the lab bench. The tube was vortexed for 5 seconds and then centrifuged at 14,000 rpm for 10 minutes. 300 µl of the supernatant was isolated in a new tube and mixed with an equal volume of isopropanol. The tubes were inverted 5-6 times to allow the supernatant and isopropanol to mix. Then, the tubes were incubated at room temperature for two minutes. The samples were centrifuged again at 14,000 rpm for 10 minutes. The supernatant was decanted, leaving the pellet in the tube. To wash the pellet, 1 mL of 70% ethanol was added to each sample, the sample was centrifuged at 14,000 for 2 minutes, and the ethanol was decanted out. The samples were placed upside down on the lab bench for 10 minutes to allow the samples to dry. Once dry, 50 µl of double distilled water was added to each sample, which could then be used for polymerase chain reactions.

2.5. RNA Extraction

An *Arabidopsis thaliana* leaf was subjected to flash freeze conditions with liquid nitrogen. The tissue of the leaf was ground up and 600 µl of trizol was added to the frozen tissue. The samples were vortexed thoroughly and then spun down via the centrifuge at 13,000 rpm for 5 minutes. The supernatant was isolated in another tube with 600 µl of 100% ethanol. Then, 600 µl of the supernatant and ethanol mixture was added to a Zymo-spin column and spun at 13,000 rpm for 1 minute. 400 µl of RNA wash buffer was added, and the samples were spun again at 13,000 rpm for 1 minute. In a separate tube, a DNase master mix (5 µl of DNase I and 75 µl of DNA digestion buffer) was made and added to the column. The mixture in the column was incubated at room temperature for 20 minutes. Then, 400 µl of RNA PreWash was added to the column and the mixture was spun down at 13,000 rpm for 1 minute. This step with the RNA PreWash was repeated twice. Afterward, 700 µl of RNA wash buffer was added to the samples, and the samples were spun down at 13,000 rpm for one minute. In a new tube, 50 µl of RNAse free water was added and left at room temperature for 1 minute. The samples were centrifuged again for one minute. Finally, the flow-through was added to the column and spun via the centrifuge.

2.6. Polymerase Chain Reaction

Template DNA from the DNA extraction was used in the polymerase chain reaction. Primers were obtained from the laboratory stock. A 20 µl PCR reaction mix was made on ice for each sample consisting of 1.0 µl of template DNA, 0.2 µl of new Taq, 2.0 µl of 10X Ex Taq Buffer, 0.5 µl of 10 mM dNTP, 0.5 µl of forward primer, 0.5 µl of reverse primer, and 15.3 µl of double distilled water. The samples were placed in a thermocycler under a specific set of conditions. The PCR conditions for DNA genotyping were 95 ºC for 5 minutes, 35 cycles x [95 ºC for 30 seconds, 55 C for 45 seconds, 72 ºC for 45 seconds], 72 ºC for seven minutes, and 4 ºC hold until the samples were removed. For RT-PCR, the PCR conditions were as follows: 95 ºC for 5 minutes, 35 cycles x [95 ºC for 30 seconds, 55 C for 30 seconds,

72 ºC for 45 seconds], 72 ºC for seven minutes, and 4 ºC hold until the samples were removed. The samples were then subjected to gel electrophoresis. 5 µl of 6X loading buffer was added to the PCR product, and then, 10 µl of the samples were placed in the wells on 1% agarose gel with ethidium bromide. In addition to the samples, 3 µl of GeneRuler 1kb plus DNA ladder was placed in a separate well. The resulting gel was viewed and pictured under a UV light.

2.7. Crystalline Cellulose Content Assay

The cell wall of four-day dark-grown hypocotyls was extracted via 40 mL of 80% ethanol. The seedlings immersed in the ethanol were placed in a water bath at 65 ºC overnight. Then, the ethanol was decanted and replaced with 40 mL of acetone. The seedlings remained overnight in acetone, and the rest of the acetone was decanted the following day. The seedlings remained in the fume hood for at least four days to dry. Once dry, the samples were ball-milled for 10 minutes and replicates were weighted using a micro-balance. For each genotype sample, five technical replicates were made. The Updegraff method was used to measure the crystalline cellulose. First, each sample was suspended in 1 mL of acetic-nitric reagent and incubated in boiling water for 30 minutes to hydrolyze the non-cellulosic polysaccharides. Once cooled, the samples were spun down at 13,000 for 10 minutes, the supernatant was decanted, the pellet was resuspended in 1mL of distilled water, and the samples were centrifuged for 10 minutes again. The supernatant was replaced with acetone, the samples were centrifuged for 10 minutes, the pellet dried overnight in the fume hood, and the pellet was hydrolyzed in 1 mL of 67% sulphuric acid overnight, with a gentle shaking from a mixing plate. Next, the anthrone assay was performed as follows: 50 µl of the solution was added to 450 µl of double distilled water, 1 mL of 0.2% anthrone was added to the samples, and the samples were incubated in boiling water for five minutes. A set of 5 glucose standards (0 µg, 5 µg, 10 ug, 25 µg, and 50 µg) were made to serve as the control group. After boiling, the tubes were

placed on ice to cool, the samples were transferred to cuvettes, and the absorbance at 620 nm was collected.

2.8. Confocal Microscopy Live Cell Imaging

Arabidopsis thaliana seeds were sterilized and grown in dark-grown conditions for 2.5 days before being subjected to 488 wavelength intensity conditions. The 2.5-day-old etiolated seedlings were mounted with double distilled water and positioned between two cover slides. A drop of immersion oil was placed on top of the cover slide to allow for better contact with the 100X lens. The Yokogawa CSUX1 spinning disk system was used to capture five-minute videos with images taken every 5 seconds to obtain a total of 61 images. Density analysis was performed on each genotype line using Dot scanner (Allen, *et al.*, 2024). For the density analysis on Dot Scanner, the lower dot threshold was set to 0.9, the upper dot threshold was 4.5, the lower blob threshold was 2.0, the dot size was 1.0, and the blob size was 5.0.

2.9. Statistical Analyses

For the hypocotyl length analyses and the crystalline cellulose content assay, a one-way ANOVA test was conducted to compare the means of each mutant to the negative control group, Col-0. The statistical difference among the means was determined by a P-value < 0.05. Regarding the density analysis, Dot scanner calculated the density of each image in YFP-CESA6 particles/μm^2. An unpaired t-test comparing the densities of the control group, YFP-CESA6 *prc1-1*, with the experimental group, YFP-CESA6 *prc1-1 tca17*, was performed. Statistical difference was determined by a two-tailed P-value < 0.05. The one-way ANOVA test and the unpaired t-test were executed using Prism 10.

Chapter 3

Results

3.1. *tca-17, rog2-2, bet3,* and *trs65* mutant lines are homozygous

When working with transgenic plants, the homozygous genotype is desirable for two reasons: it ensures that the mutant allele is being passed down to future generations and that the mutant allele is the only allele contributing to the phenotype. Thus, prior to looking for any deficiencies in cellulose-related phenotypes, a DNA genotype analysis was performed on four mutant lines — *tca17, rog2-2, bet3,* and *trs65* — to confirm homozygosity (Figure 3). Each mutant was compared to a negative control group, the wild type (WT) band. The leftmost bands in the gel represent the DNA ladder with the 1500 base pairs and 500 base pairs markers indicated to allow for comparison and identification of the transfer DNA (T-DNA) band containing the insertion mutation.

Each mutant had distinct bands from the WT band, indicating that all four of the mutants are homozygous lines. As seen in Figure 3A, *tca17* had bands between 500-1000 bp, *rog2-2* (also known as TRAPPC11) had bands between 700-1000 bp, *trs65* had a band close to the 500 bp marker, and *bet3* had bands at 500-700 bp (Figure 3A). The location of each mutant in their genes, the primers used for each mutant, and the length of the DNA sequence for the WT and T-DNA band are presented in Figure 3B (Figure 3B). Each mutant produced WT and T-DNA band lengths that fall within the expected range for the primers used indicated in Figure 3B.

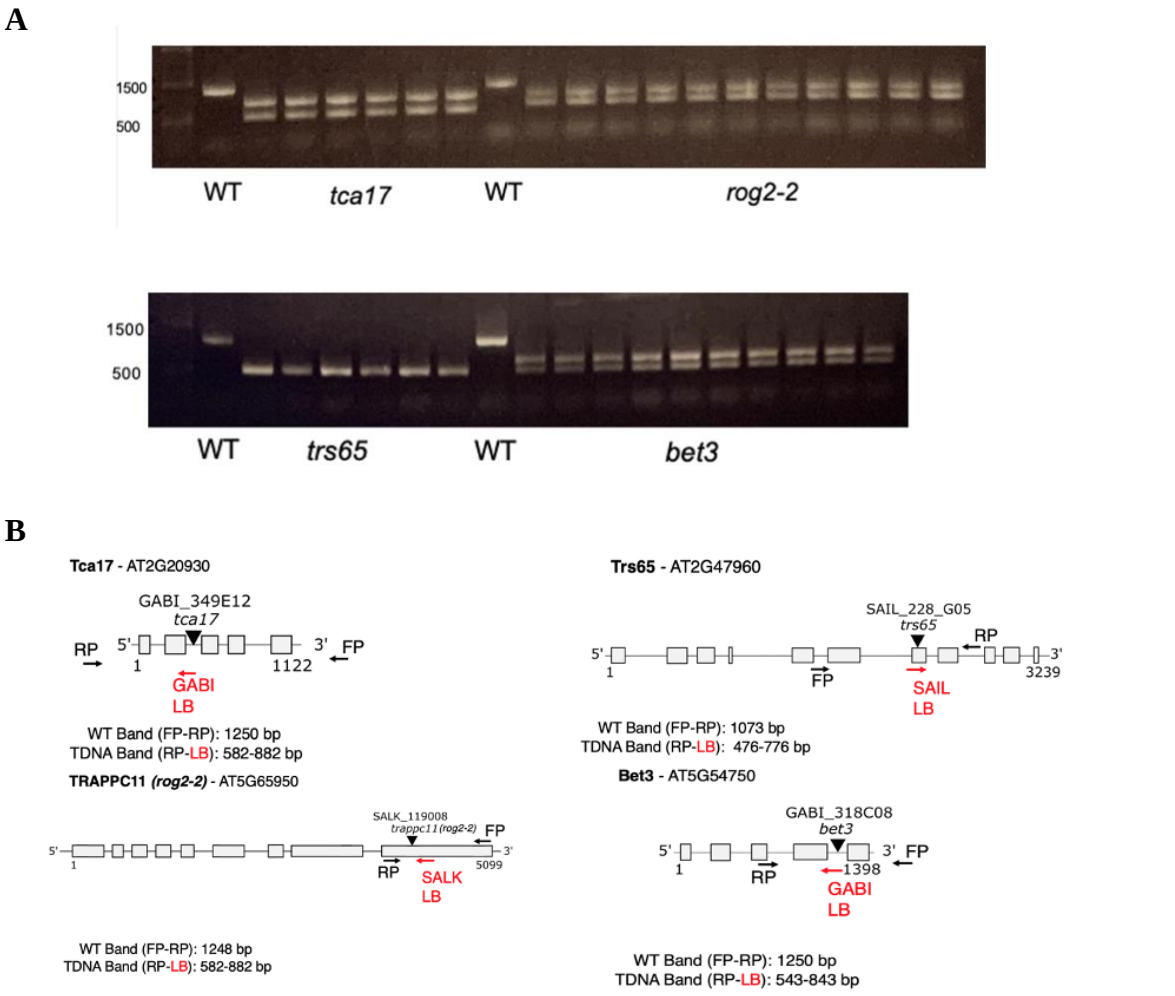

Figure 3. DNA Genotype and Primers for Four Mutant DNA Lines

(A) The top gel contains the DNA genotype for *tca17* and *rog2-2* while the bottom gel contains the DNA genotype for *trs65* and *bet3*. For both gels, the leftmost well contains the DNA gel ladder to determine the size of the WT and T-DNA bands. WT bands are used for each gene to determine homozygosity. (B). The specific primers used, the location of the insertion mutation, the length of the wild type (WT) band from the forward primer (FP) and the reverse primer (RP), and the length of the transgenic DNA band (T-DNA) band from the RP to the left-border primer (LB) for each of the mutant lines are shown in this figure.

3.2. The hypocotyl length for *bet3*, *rog2-2*, and *tca-17* etiolated seedlings are reduced at seven days

Under dark-grown conditions, CESAs required for cellulose synthesis may be affected, resulting in reduced hypocotyl lengths (Hill *et al*., 2018). Therefore, to determine if a cellulose-related phenotype exists in *bet3*, *rog2-2*, *tca-17*, or *trs65* mutants, the hypocotyl lengths of etiolated seedlings were analyzed. If the mutant hypocotyl length is similar to Col-0, then the insertion mutation compliments the wild type phenotype, suggesting that the insertion mutation does not affect the hypocotyls' growth under dark-grown conditions. However, if the mutant hypocotyl length is significantly different from the Col-0, the insertion mutation causes a cellulose-related phenotype. Cellulose Synthase-Interactive Protein 1 (*csi1-3)* interacts with CESA6 and has reduced hypocotyl growth under dark-grown conditions (Gu *et al*., 2010). It is the positive control group that should be statistically different from Col-0, indicating the validity of the results obtained.

For each mutant, the hypocotyl length of four-day-old etiolated seedlings and seven-day-old etiolated seedlings was analyzed (Figure 4). At four days, the hypocotyl lengths for all of the mutants were not statistically different from Col-0 (Figure 4A). However, at seven days, *bet3*, *rog2-2*, and *tca17* showed statistically significant reduced hypocotyl lengths from Col-0 with *tca17* having the greatest reduction (Figure 4B). Although *trs65* displayed slightly lower lengths than Col-0, the difference was not statistically significant, suggesting that the hypocotyl growth in *trs65* is unaffected at both four days and seven days (Figure 4A and 4B).

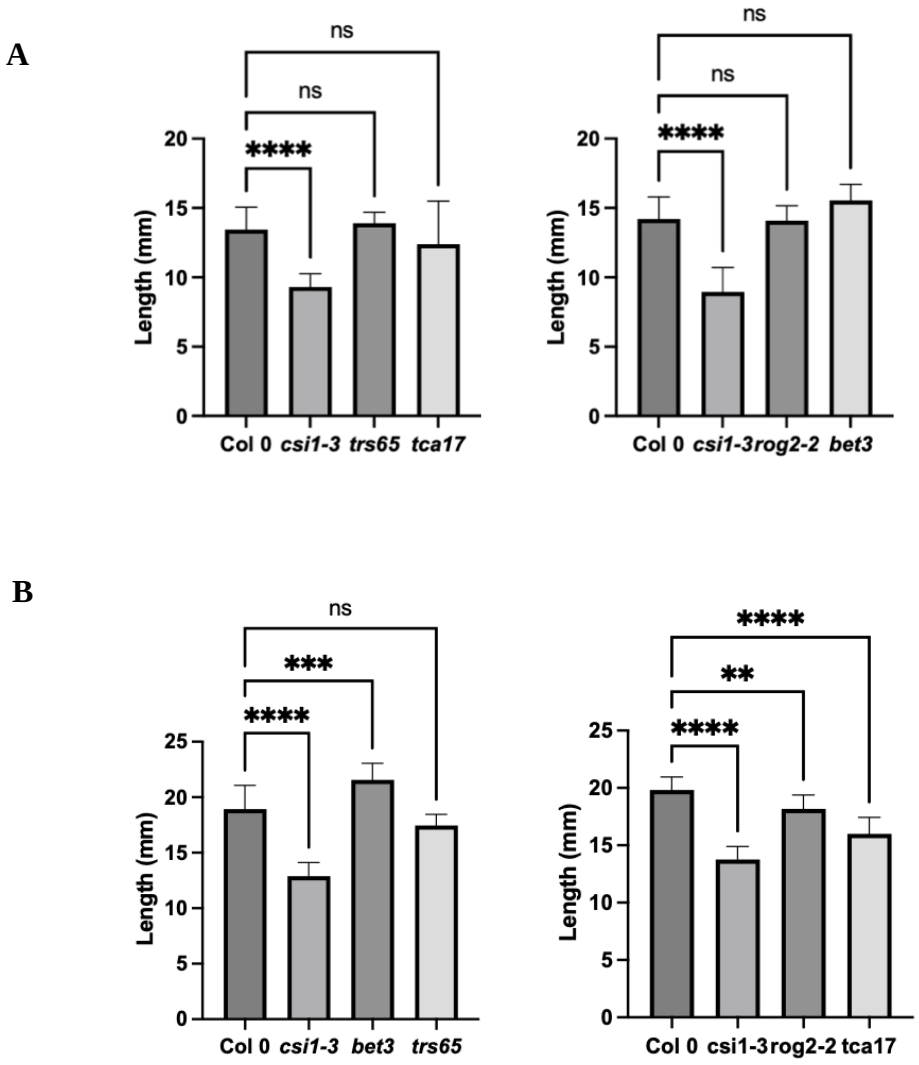

Figure 4. Four-Day and Seven-Day Dark-Grown Hypocotyl Lengths

(A) Four-day hypocotyl lengths for *trs65* and *tca17* (left graph) and *rog2-2* and *bet3* (right graph) are compared to the wild type (Col-0). *csi1-3* is the positive control. The asterisks and ns (not significant) above the bars indicate degrees of significance based on a one-way ANOVA test ($P \leq 0.05$). The more asterisks, the greater the significance. (B) Seven-day hypocotyl lengths for *bet3* and *trs65* (left graph) and *rog2-2* and *tca17* (right graph) are compared to Col-0.

3.3. *tca17*, *rog2-2*, and *trs65* are knockout mutants

A gene expression analysis for *tca17*, *rog2-2*, *trs65*, and *bet3* was performed to test whether any cellulose-related phenotypic results observed, such as a smaller hypocotyl length, were due to transcriptional differences. Each of the mutants was compared to the wild type (Col-0) because it does not contain the specific insertion mutations. Actin was also used as a control to make sure that the cDNA was present and that the concentration levels of the cDNA were the same (Figure 5A). It is important to have constant concentration levels to ensure that the expression of the gene is only influenced by the insertion mutation.

The *tca17* insertion mutation is near the beginning of the gene, and thus gene expression was analyzed using primers downstream from the mutation (Figure 5B). For each mutation, three replicates were made and compared against three wild type replicates. No gene expression band showed for *tca17*, thus indicating that it is a knockout mutation (Figure 5A). For Trs65, the *trs65* mutation is located approximately two-thirds of the way through the gene. As a result, gene expression was analyzed with primers both upstream and downstream from the mutation (Figure 5B). At both locations, no gene expression band was observed, indicating a loss of gene expression due to the mutation (Figure 5A). For Rog2-2 and Bet3, the entire length of the genes was analyzed using the FP at the upstream location and the RP from the downstream location as indicated in Figure 5B with the blue circles (Figure 5B). For *rog2-2*, no gene expression bands showed, indicating a knockout mutation (Figure 5A). However, for *bet3*, bands similar to the WT bands were observed. The *bet3* insertion mutation did not affect gene expression levels (Figure 5A).

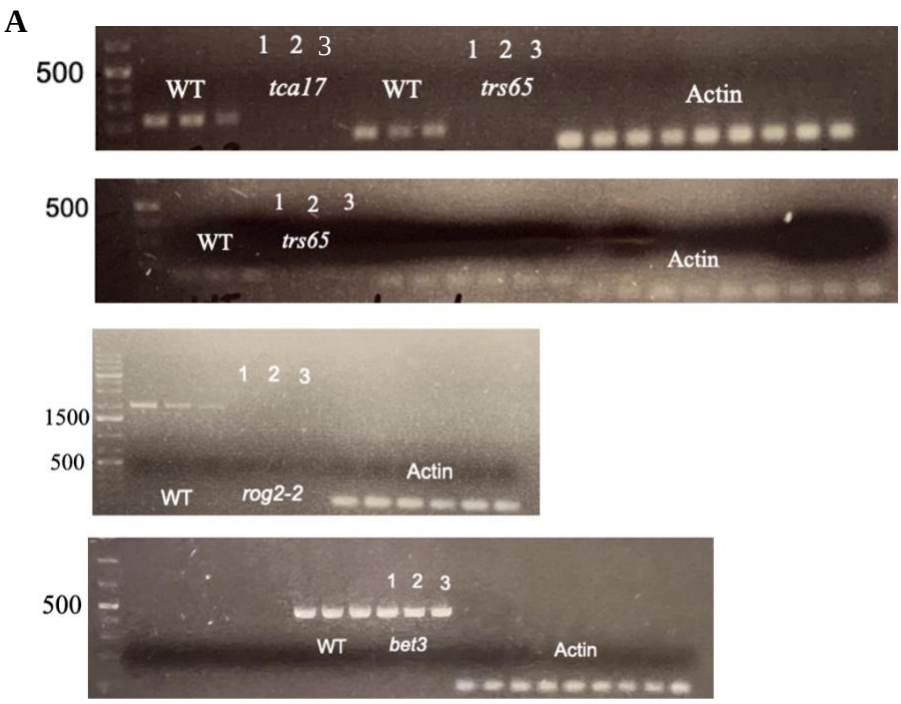

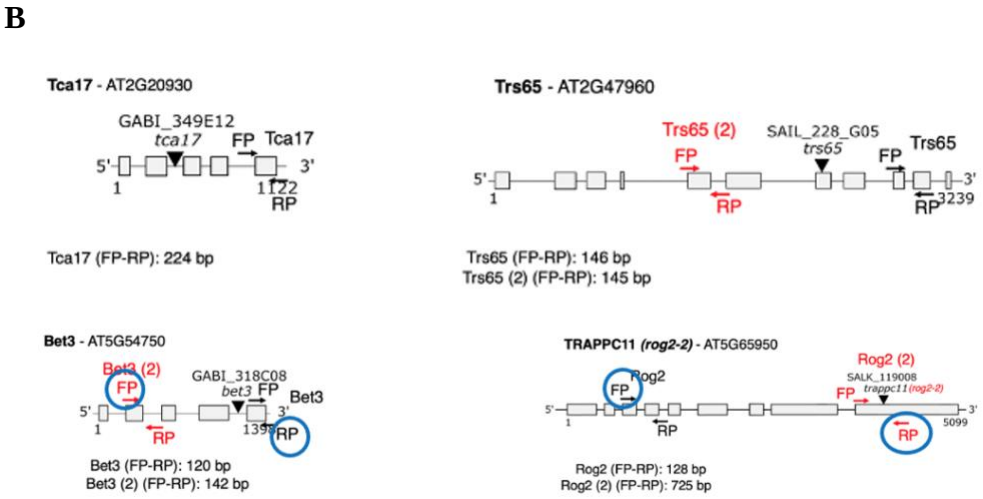

Figure 5. RNA Expression for *tca17*, *trs65*, *rog2-2*, and *bet3*

(A) The top gel shows the gene expression for *tca17*, and the gene expression with the downstream primers for *trs65*. The downstream primers are the black FP and RP primers indicated in Figure 5B. The second gel shows the gene expression with the upstream primers (in red in Figure 5B) for *trs65*. The third gel shows the full-length gene expression for *rog2-2*, and the fourth gel is the gene expression for the full length of *bet3*. The leftmost well contains the

DNA gel ladder with the 500 bp and 1500 bp markers labeled to determine the size of the gene expression band. (B) The location of the insertion mutation, the FP and RP used to determine the gene expression, and the length of the expected band are shown in this figure.

3.4. Cellulose content is reduced in the tca17 primary cell wall

As previously observed, *tca17* and *rog2-2* both had reduced hypocotyl lengths at seven days. To investigate whether Tca17 and Rog2-2 play a role in cellulose synthesis, a crystalline cellulose content assay on four-day-old etiolated hypocotyls was performed. Even though the reduced hypocotyl length was observed at seven days, the cellulose content was still analyzed at four days. It is assumed that if the cellulose content is reduced at four days, there will still be a reduction of cellulose in the mutants at seven days. As shown in Figure 6, *tca17* had a significantly lower cellulose content than Col-0 (Figure 6). The *rog2-2* mutant had similar cellulose content levels with Col-0, which were not statistically significant (Figure 6).

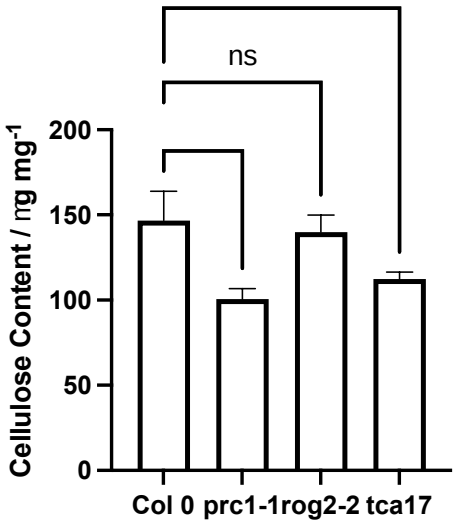

Figure 6. Four-Day Cellulose Content for *rog2-2* and *tca17*

The crystalline cellulose content levels for *rog2-2* and *tca17* were measured in four-day-old etiolated hypocotyls and compared to Col-0, the negative control. The positive control was *prc1-*

1. The statistical significance is indicated by the asterisks and ns (no significance) above each bar based on a one-way ANOVA test ($P \leq 0.05$). A higher number of asterisks represents a higher statistical significance.

3.5. The density of CESA6 particles at the PM was not affected in *tca17*

To further investigate the role of Tca17 in cellulose synthesis in the primary cell wall, the density of yellow fluorescent tagged CESA6 proteins (YFP-CESA6) was measured in *prc1-1* and *prc1-1 tca17* backgrounds. YFP-CESA6 complements the *prc1-1* mutation, and thus YFP-CESA6 *prc1-1* is a frequent fluorescent marker used to assess the dynamics, regulation, and trafficking of CSCs at the plasma membrane (Allen *et al.*, 2024b). It serves as the control group. The YFP-CESA6 plasma membrane density can determine if there is a disruption in the delivery or removal of the CSCs from the plasma membrane (Allen *et al.*, 2024b). In *prc1-1 tca17*, the density of YFP-CESA6 was slightly lower than *prc1-1*, however, the slight reduction was not statistically significant as indicated by a t-test with a P value ≤ 0.05 (Figure 7). Therefore, the density of YFP-CESA6 at the plasma membrane was similar in *prc1-1* and *prc1-1 tca17.*

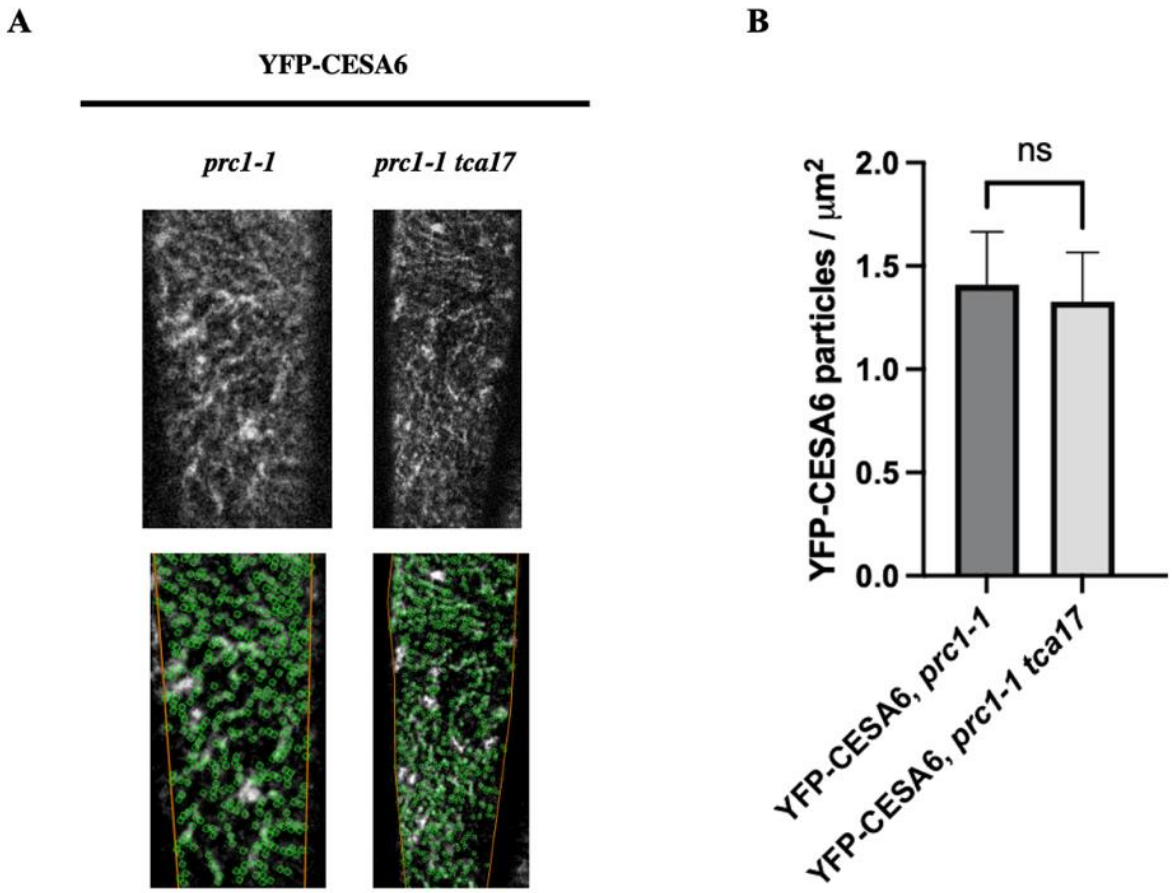

Figure 7. YFP-CESA6 particle density for *tca17*

(A) Representative raw (top panel) and analyzed (bottom panel) images of YFP-CESA6 at the plasma membrane in *prc1-1* (control) background and *prc1-1 tca17* (experimental) background in 2.5-day-old dark-grown hypocotyls. For the bottom panel, the green dots represent CESA6 particles. (B) The YFP-CESA6 particle density (n=15 images) for the *prc1-1* and *prc1-1 tca17* background. The ns above the graphs indicate no significance between the two groups based on a t-test ($P \leq 0.05$).

Chapter 4

Discussion

4.1. Analysis of Preliminary Data

The DNA genotyping, dark-grown hypocotyl length, RNA expression, and crystalline cellulose content assay results were preliminary data used to identify *tca17*'s cellulose-related phenotypes and further investigate its role in the TRAPP complex and CSC trafficking to the plasma membrane (PM). The genotype was first determined for each of the mutants to check for homozygous lines. All four mutant lines displayed homozygosity since the T-DNA bands were different from the wild type bands. For homozygous lines, it is expected that only one band should appear in the gel; however, *tca17*, *rog2-2*, and *bet3* all had two bands appear. The second band may be other DNA within the sample since the DNA extraction method is not as precise at extracting out solely the desired DNA.

Upon confirming that the mutants were homozygous, the hypocotyl length of four-day-old and seven-day-old seedlings were measured. There was no significant reduction in the hypocotyl length for any of the mutants at four days. However, for seven-day-old etiolated hypocotyls, *rog2-2*, *tca17*, and *bet3* all had reduced hypocotyl lengths. The insertion mutation may not be as severe in these three mutant backgrounds since it took longer to observe the reduction in hypocotyl length.

To explain the cellulose-related phenotype of smaller hypocotyls observed for *rog2-2*, *tca17*, and *bet3*, the gene expression of each mutant line was obtained. *Rog2-2*, *tca17*, and *trs65* were knockout mutations, indicating that the insertion mutation causes the gene to lose its expression. This loss of expression could explain the reduction in hypocotyl length observed in *tca17* and *rog2-2*. Even though the *trs65* hypocotyl length was similar to Col-0, Trs65 was a knockout gene. Thus, the insertion mutation may biologically affect *Arabidopsis thaliana* in a way unrelated to cellulose synthesis. Because Bet3 showed no disturbance in gene expression, it is equivalent to Col-0.

Out of the four mutants, *tca17* and *rog2-2* were shown to be the most promising in being involved in cellulose synthesis. Both mutants have reduced hypocotyl lengths and loss of gene expression. As a result, a crystalline cellulose content assay was performed on *tca17* and *rog2-2* only. A statistically significant lower cellulose content would indicate that the insertion mutation is causing a disruption in the cellulose synthesis pathway, and thus the subunit is important for the proper synthesis pathway. The cellulose content was significantly reduced in *tca17*. Consequently, the research shifted towards focusing on the subcellular dynamics of YFP-CESA6 particles in the *tca17* background.

4.2. Comparison of *prc1-1 tca17* density data with *prc1-1 trs85-1*

Trs85 is a specific subunit within the TRAPPIII complex, which is thought to be involved in the autophagy process in plants. Previous research on Trs85 revealed that the subunit directly interacts with CSI1 (Allen *et al*, 2024b). The delivery of CSCs to the PM is directed by cortical microtubules, and CSI1 has been shown to serve as a link between CSCs and microtubule interactions (Zhu *et al.*, 2018). Thus, the interaction between CSI1 and Trs85 suggests that this specific subunit is involved in CSC trafficking. Further research on Trs85 revealed that the *trs85-1* mutant has a reduced dark-grown hypocotyl and a lower crystalline cellulose content in four-day-old hypocotyls (Allen *et al*, 2024b). Both phenotypes are cellulose-related phenotypes and are indicative of a disruption to the cellulose synthesis in the primary cell well in the absence of Trs85. The density of YFP-CESA6 particles in the *prc1-1 trs85-1* mutant background was significantly increased by 14% in 2.5-day-old dark-grown hypocotyl, indicating an increase in secretion of CSC to the PM or a disruption in the internalization of CSC into small cellulose synthase compartments (SmaCCs) and microtubules associated SmaCCS (MASCs) (Allen *et al*, 2024b). SmaCCs/MASCs function in recycling CSCs back to the PM (Allen *et al*, 2021). The velocity of the YFP-CESA6 particles at the plasma membrane in the *prc1-1 trs85-1* mutant was significantly reduced by approximately 20% in comparison to *prc1-1*. A slower velocity of the YFP-CESA6 particles could

indicate a decrease in the synthesis of cellulose microfibrils at the plasma membrane and thus could explain the reduction in cellulose content in four-day-old dark-grown hypocotyls (Allen *et al*, 2024b). Overall, Trs85 is thought to play a role in the endocytosis and exocytosis of CSC, making it an important subunit for the trafficking and regulation of CSCs at the plasma membrane.

The preliminary data for Tca17, a TRAPPII and TRAPPIII specific subunit, showed that it also had a shorter dark-grown hypocotyl length at seven days, as opposed to four days, and a reduced crystalline cellulose content in four-day-old hypocotyls. Given similar cellulose-related phenotypes with Trs85 and their association within the TRAPPIII complexes, it was hypothesized that Tca17 might function similarly in endocytosis and exocytosis of CSC or interact with Trs85. However, the YFP-CESA6 particle density in the *prc1-1 tca17* mutant was comparable to the *prc1-1* mutants, suggesting no significant impact. The absence of the Tca17 subunit most likely does not cause an increase of CSC to the PM or a decrease in the CSC internalization, thus leading to the possibility that Tca17 and Trs85 have independent roles in cellulose synthesis.

While live-cell five-minute videos were taken on *prc1-1* and *prc1-1 tca17* 2.5-day-old etiolated hypocotyls, the videos were not clear and focused to analyze and get an accurate representation of the YFP-CESA6 particle velocity in both backgrounds. Therefore, moving forward, the velocity of YFP-CESA6 particles at the plasma membrane for *prc1-1 tca17* should be taken and analyzed to elucidate if the particles' velocity behaves similarly to *prc1-1 trs85-1*. If a decrease in velocity is observed, it could explain the lower crystalline cellulose content and could suggest that Tca17 plays a role in regulating the CSC catalytic activity of synthesizing cellulose microfibrils. In this case, Tca17 may act similarly to Trs85 while also having other independent functions relating to cellulose synthesis.

4.3. Conclusion

In this research project, four TRAPPII or TRAPPIII specific subunits were investigated to determine if any of the subunits played a role in cellulose synthesis. Through the dark-grown hypocotyl experiment, the RNA expression, and the crystalline cellulose content assay, Tca17 is thought to most likely be involved in cellulose synthesis at the PM in *Arabidopsis thaliana*. It had a reduced hypocotyl length at seven days and a lower crystalline cellulose content at four days, both of which are phenotypes indicative of a disruption in the cellulose synthesis pathway. To further investigate its role in cellulose synthesis, the density of the *tca17* mutant was observed in the *prc1-1 tca17* background and compared to *prc1-1 trs85-1* to see if the Tca17 subunit functions similarly to Trs85. Trs85 had a higher YFP-CESA6 density, suggesting that Trs85 is important in the endocytosis and exocytosis of CSC at the PM. The YFP-CESA6 density in *prc1-1 tca17* was similar to *prc1-1*. Therefore, while Tca17 may still play an important role in the cellulose synthesis pathway, it may function differently than the Trs85 subunit. In the future, more experimentation on the YFP-CESA6 dynamics, such as the velocity of the particles and the delivery rate of the particles, in the *prc1-1 tca17*, can be performed to gain a better understanding of Tca17's role in the cellulose synthesis pathway.

BIBLIOGRAPHY

Allen, H., Davis, B., Patel, J., & Gu, Y. (2024). Dot Scanner: Open-source software for quantitative live-cell imaging in Planta. *The Plant Journal*. =-https://doi.org/10.1111/tpj.16662

Allen, H., Wei, D., Gu, Y., & Li, S. (2021). A historical perspective on the regulation of cellulose biosynthesis. *Carbohydrate Polymers*, *252*, 117022. https://doi.org/10.1016/j.carbpol.2020.117022

Allen, H., Zhu, X., Li, S., & Gu, Y. (2024b). The TRAPPIII subunit, TRS85, has a dual role in the trafficking of cellulose synthase complexes in *Arabidopsis*. *The Plant Journal*. https://doi.org/10.1111/tpj.16688

Barrowman, J., Bhandari, D., Reinisch, K., & Ferro-Novick, S. (2010). Trapp complexes in membrane traffic: Convergence through a common rab. *Nature Reviews Molecular Cell Biology*, *11*(11), 759–763. https://doi.org/10.1038/nrm2999

Endler, A., Kesten, C., Schneider, R., Zhang, Y., Ivakov, A., Froehlich, A., Funke, N., & Persson, S. (2015). A mechanism for sustained cellulose synthesis during salt stress. *Cell*, *162*(6), 1353–1364. https://doi.org/10.1016/j.cell.2015.08.028

Ezquer, I., Salameh, I., Colombo, L., & Kalaitzis, P. (2020). Plant Cell Walls Tackling Climate Change: Biotechnological strategies to improve crop adaptations and photosynthesis in response to global warming. *Plants*, *9*(2), 212. https://doi.org/10.3390/plants9020212

Gu, Y., Kaplinsky, N., Bringmann, M., Cobb, A., Sampathkumar, A., Baskin, T. I., Persson, S., & Somerville, C. R. (2010). Identification of a cellulose synthase-associated protein required for cellulose biosynthesis. *Proceedings of the National Academy of Sciences*, *107*, 12866–12871. https://doi.org/10.1073/pnas.1007092107

Hill, J. L., Josephs, C., Barnes, W. J., Anderson, C. T., & Tien, M. (2018). Longevity in vivo of primary cell wall cellulose synthases. *Plant Molecular Biology*, *96*(3), 279–289. https://doi.org/10.1007/s11103-017-0695-4

Kim, J. J., Lipatova, Z., & Segev, N. (2016). Trapp complexes in secretion and autophagy. *Frontiers in Cell and Developmental Biology*, *4*. https://doi.org/10.3389/fcell.2016.00020

Lei, L., Singh, A., Bashline, L., Li, S., Yingling, Y. G., & Gu, Y. (2015). Cellulose synthase Interactive1 is required for fast recycling of cellulose synthase complexes to the plasma membrane in *Arabidopsis*. *The Plant Cell*. https://doi.org/10.1105/tpc.15.00442

Montpetit, B., & Conibear, E. (2009). Identification of the novel Trapp Associated Protein TCA17. *Traffic*, *10*(6), 713–723. https://doi.org/10.1111/j.1600-0854.2009.00895.x

Ravikumar, R., Steiner, A., & Assaad, F. F. (2017). Multisubunit tethering complexes in higher plants. *Current Opinion in Plant Biology*, *40*, 97–105. https://doi.org/10.1016/j.pbi.2017.08.009

Zhang, Y., Nikolovski, N., Sorieul, M., Vellosillo, T., McFarlane, H. E., Dupree, R., Kesten, C., Schneider, R., Driemeier, C., Lathe, R., Lampugnani, E., Yu, X., Ivakov, A., Doblin, M. S., Mortimer, J. C., Brown, S. P., Persson, S., & Dupree, P. (2016). Golgi-localized stello

proteins regulate the assembly and trafficking of cellulose synthase complexes in *Arabidopsis*. *Nature Communications, 7*(1). https://doi.org/10.1038/ncomms11656

Zhu, X., Li, S., Pan, S., Xin, X., & Gu, Y. (2018). CSI1, PATROL1, and exocyst complex cooperate in delivery of cellulose synthase complexes to the plasma membrane. *Proceedings of the National Academy of Sciences*, *115*(15). https://doi.org/10.1073/pnas.1800182115